

Novel ideas in nonleptonic decays of double heavy baryons

Thomas Gutsche¹, Mikhail A. Ivanov², Jürgen G. Körner³, Valery E. Lyubovitskij^{1,4}

¹ Institut für Theoretische Physik, Universität Tübingen, Kepler Center for Astro and Particle Physics, Auf der Morgenstelle 14, D-72076 Tübingen, Germany

² Bogoliubov Laboratory of Theoretical Physics, Joint Institute for Nuclear Research, 141980 Dubna, Russia

³ PRISMA⁺ Cluster of Excellence, Institut für Physik, Johannes Gutenberg-Universität, D-55099 Mainz, Germany

⁴ Departamento de Física y Centro Científico Tecnológico de Valparaíso-CCTVal, Universidad Técnica Federico Santa María, Casilla 110-V, Valparaíso, Chile

* Correspondence: valeri.lyubovitskij@uni-tuebingen.de

Received: 15 May 2019; Accepted: 10 June 2019; Published: 13 June 2019

Abstract: The recent discovery of double charm baryon states by the LHCb Collaboration and their high precision mass determination calls for a comprehensive analysis of the nonleptonic decays of double and single heavy baryons. Nonleptonic baryon decays play an important role in particle phenomenology since they allow to study the interplay of long and short distance dynamics of the Standard Model (SM). Further, they allow one to search for New Physics effects beyond the SM. We review recent progress in experimental and theoretical studies of the nonleptonic decays of heavy baryons with a focus on double charm baryon states and their decays. In particular, we discuss new ideas proposed by the present authors to calculate the W -exchange matrix elements of the nonleptonic decays of double heavy baryons. An important ingredient in our approach is the compositeness condition of Salam and Weinberg, and an effective implementation of infrared confinement both of which allow one to describe the nonperturbative structure of baryons composed of light and heavy quarks. Further we discuss an *ab initio* calculational method for the treatment of the so-called W -exchange diagrams generated by W^\pm boson exchange between quarks. We found that the W^\pm -exchange contributions are not suppressed in comparison with the tree-level (factorizing) diagrams and must be taken into account in the evaluation of matrix elements. Moreover, there are decay processes such as the doubly Cabibbo-suppressed decay $\Xi_c^+ \rightarrow p\phi$ recently observed by the LHCb Collaboration which is contributed to only by one single W -exchange diagram.

Keywords: heavy baryons, light and heavy quark, hadronization, confinement, covariant constituent quark model, nonleptonic decays

Foreword

This paper is written in memory of Garry Efimov (1934–2015). For two of us (Mikhail Ivanov and Valery Lyubovitskij) Garry Efimov was a teacher and subsequently an important collaborator. He significantly contributed to the development of nonlocal quantum field theory and its relation to hadron structure. In particular, he showed that the nonlocal structure of hadron-quark interactions is important for a realistic description of the nonperturbative features of the strong interaction contributions at large distances. Phenomena such as hadronization and confinement can be consistently implemented in field-theoretical approaches based on nonlocal phenomenological Lagrangians. Garry Efimov with his pupils and collaborators developed a series of relativistic quark models based on nonlocal Lagrangians.

The covariant constituent quark model (CCQM) developed by us and described in the present paper is deeply rooted in his ground-breaking ideas on the use of nonlocal quantum field theory in particle physics.

1. Introduction

The nonleptonic decays of light and especially heavy baryons play an important role in the phenomenology of particle interactions. The nonleptonic decays can be used to determine some of the parameters of the Standard Model (SM) and to search for New Physics beyond the SM. The last decades have seen significant experimental progress in the study of nonleptonic decays of heavy baryons. The CDF, ATLAS, LHCb, Belle and BES Collaborations have measured various features of the nonleptonic decays of heavy baryons [1]. In particular, there are now more precise results on the branching ratios of the two-body decays of charm baryons $\Lambda_c^+ \rightarrow p\phi, \Lambda\pi^+, \Sigma^+\pi^0$ [2] and $\Xi_c^+ \rightarrow p\bar{K}^*(892)^0$ [3], and bottom baryons $\Lambda_b^0 \rightarrow \Lambda J/\psi, \Lambda\psi(2S)$ [4,5]. Starting in 2005 a new era began in the studies of double charm baryons when the SELEX Collaboration reported on the observation of a state with the quantum numbers of the spin 1/2 ground state Ξ_{cc}^+ baryon with a mass of 3518 ± 3 MeV [6]. This double charm baryon state was conjectured to be an isospin- $\frac{1}{2}$ baryon with quark content (dcc) and to have an isospin partner Ξ_{cc}^{++} with the quark structure (ucc). However, other Collaborations (BABAR, Belle, LHCb [1]) found no evidence for the Ξ_{cc}^+ nor the Ξ_{cc}^{++} states in the conjectured mass region of ~ 3500 MeV. Recently the LHCb Collaboration discovered the double charm state Ξ_{cc}^{++} [7]-[9] in the invariant mass spectrum of the final state particles ($\Lambda_c^+ K^- \pi^+ \pi^+$). The extracted mass of the Ξ_{cc}^{++} state was given as $3621.40 \pm 0.72 \pm 0.27 \pm 0.14$ MeV and was ~ 100 MeV heavier than the mass of the original SELEX double charm baryon state Ξ_{cc}^+ which made it quite unlikely that the two states were isospin partners. On the other hand, the LHCb mass measurement was in agreement with theoretical mass value predictions for the double charm baryon states. In particular, the central mass value of the LHCb result for the Ξ_{cc}^{++} was very close the value 3610 MeV and 3620 MeV predicted in [10,11] using the one gluon exchange model of de Rujula, Georgi and Glashow [12] and a relativistic quark-diquark potential model [13], respectively. Fleck and Richard using a variety of models had also predicted a mass value of ~ 3600 [14] while Karliner et al. found $M_{\Xi_{cc}^+} = 3627 \pm 12$ MeV [15].

The new measurement of the LHCb Collaboration has stimulated much theoretical activity concerning the structure of the nonleptonic decays of double heavy baryons. The nonleptonic two-body baryon decays can be conveniently classified by the color-flavor quark level topologies with a single effective W -exchange between the constituent quarks participating in the decay process. The corresponding set of topological quark diagrams are shown in Fig. 1. They can be divided into two subgroups: i) the reducible so-called tree-diagrams Ia and Ib, and ii) the irreducible W -exchange diagrams IIa, IIb and III. Further details can be found in Ref. [10,11,16,17]. The tree-diagrams Ia and Ib can be factorized into the lepton decay of the emitted meson and a baryon-baryon transition matrix element induced by the relevant weak currents. The W -exchange diagrams IIa, IIb and III are more difficult to evaluate from first principles.

The two-body nonleptonic decays of the double charm baryon states $\Xi_{cc}^{+,++}$ were studied in Ref. [18] by using factorization for the tree diagrams and a pole model for the W -exchange contributions. The nonfactorizable W -exchange contributions obtained in their pole model approach were found to be sizable and provide an indication that the W -exchange contributions cannot be ignored. In Ref. [19] the same approach has been applied to the nonleptonic decay modes of the double charm strange Ω_{cc}^+ baryon. It was found that the branching ratios of some of the nonleptonic Ω_{cc}^+ decay modes obtain contributions solely from W -exchange diagrams, resulting in branching ratios as large as $\sim \mathcal{O}(10^{-2})$. The W -exchange contributions in double charm decays have been found to be comparable to the factorizable contributions

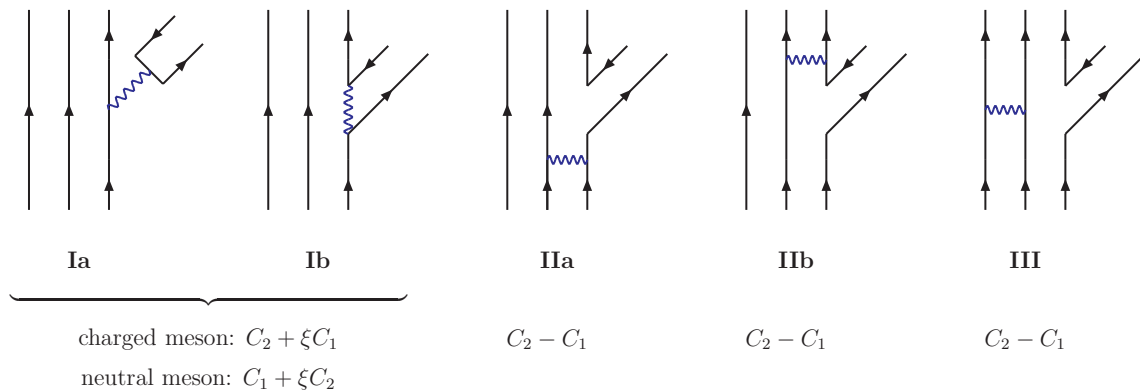


Figure 1. Flavor-color topologies of nonleptonic two-body decays.

for most of the decay modes. In the paper by Zhang et al. [20] the W -exchange contributions have been analyzed for the nonleptonic transitions of the double heavy baryon states Ξ_{bc} and Ω_{bc} using $SU(3)$ flavor symmetry. The decay amplitudes for the various decay channels were parameterized in terms of $SU(3)$ irreducible amplitudes resulting in a number of relations between the decay widths. In Ref. [21] various nonleptonic decay modes of double charm, bottom-charm, and double bottom baryons have been analyzed using a light-front QCD approach for the calculation of hadronic form factors induced by the $c \rightarrow d(s)$ and $b \rightarrow u(c)$ quark-level transitions. A detailed theoretical analysis of the production, lifetime and semileptonic and nonleptonic decays of double heavy baryons has been performed in Refs. [22,23] by using nonrelativistic QCD. The analysis resulted in a number of predictions for various exclusive decay modes (nonleptonic modes with π , ρ mesons in the final state and semileptonic modes). The authors of Ref. [24] studied the nonleptonic decays of double charm baryon into single charm baryons and light vector mesons in a phenomenological approach based on the factorization hypothesis to evaluate short-distance effects, while long-distance effects were modelled as final-state interactions and were estimated using a one-particle-exchange model.

Our group has been studying nonleptonic decays of both single and double heavy baryons for a number of years [25]-[32]. Use was made of a covariant constituent quark model (CCQM) based on phenomenological nonlocal Lagrangians describing the coupling of single and double heavy baryons to their constituent quarks. Common to all our studies is the use of the Weinberg-Salam compositeness condition formulated in Refs. [33]-[36]. The compositeness condition allows one to determine the coupling constant between the hadrons and their constituent quarks. The compositeness condition has been successfully applied to the description of a variety of hadrons and exotic states such as tetraquarks and hadronic molecules (see, e.g., Refs. [36]-[42]). In the later versions of our covariant constituent quark model we have implemented the infrared (IR) confinement of quarks by a cut in the relevant scale integration at a value $\lambda_{\text{IR}} = 181$ MeV. The infrared cut-off was taken to be universal for all processes considered in this approach.

Let us review our results on the nonleptonic decays of heavy baryons described in [25]-[32] in more detail. In a 1998 precursor to the present version of the CCQM model we presented a comprehensive analysis of heavy-to-heavy and heavy-to-light nonleptonic transitions involving spin- $\frac{1}{2}$ baryons [25,26]. Instead of using full dynamic quark propagators we employed static approximations for the light quark $q = u, d, s$ propagators and leading-order contributions for the heavy quark $Q = c, b$ propagators in the $1/m_{c/b}$ expansion, i.e. in the heavy quark limit. We included the factorizing tree diagrams as well as the nonfactorizing W -exchange contributions to the decay amplitudes. We found that for heavy-to-light

transitions $Q \rightarrow qud$ the total contribution of the nonfactorizing diagrams amounted up to $\sim 60\%$ of the factorizing contributions in amplitude, and up to $\sim 30\%$ for $b \rightarrow c\bar{u}d$ transitions. We calculated the rates and polarization parameters for various nonleptonic modes of baryons and compared them to data and existing theoretical predictions.

In Ref. [27] we calculated the invariant and helicity amplitudes for the nonleptonic decay $\Lambda_b \rightarrow \Lambda + J/\psi, \psi(2S)$ in the CCQM model. We discussed joint angular decay distributions in the cascade decay $\Lambda_b \rightarrow \Lambda(\rightarrow p\pi^-) + J/\psi, \psi(2S)(\rightarrow \ell^+\ell^-)$ and calculated some of the asymmetry parameters characterizing the joint angular decay distribution. We confirmed expectations from the naive quark model that the transitions into the $\lambda_\Lambda = 1/2$ helicity states of the daughter baryon Λ are strongly suppressed leading to a near maximal negative polarization of the Λ . For the same reason the azimuthal correlation between the two decay planes spanned by $(p\pi^-)$ and $(\ell^+\ell^-)$ is negligibly small. We provided form factor results for the whole accessible range of q^2 -values. Our results were found to be close to lattice QCD results at minimum recoil and light-cone QCD sum rule results at maximum recoil. A new feature of our analysis was that we included lepton mass effects in the calculation which allowed us also to describe the cascade decay $\Lambda_b \rightarrow \Lambda(\rightarrow p\pi^-) + \psi(2S)(\rightarrow \tau^+\tau^-)$. Our prediction for the branching ratio $R(\Lambda_b) = \Gamma(\Lambda_b^0 \rightarrow \psi(2S)\Lambda^0)/\Gamma(\Lambda_b^0 \rightarrow J/\psi\Lambda^0) = 0.8 \pm 0.1$ differed from the measured branching ratio $R(\Lambda_b) = 0.501 \pm 0.033(\text{stat}) \pm 0.019(\text{syst})$ by the ATLAS Collaboration [5] by 2.8 standard deviations.

In Ref. [28] we presented a detailed analysis of the above branching ratio $R(\Lambda_b)$ using a model-independent framework for the heavy-to-light form factors in which the values of the form factors grow when going from $q^2 = m^2(J/\psi)$ to $q^2 = m^2(\psi(2S))$. Taking into account phase-space suppression effects as well as the difference of the leptonic decay constants $f_{J/\psi}$ and $f_{\psi(2S)}$ we obtained $R(\Lambda_b) = 0.81$ in agreement with our previous result published in Ref. [28]. The small $R(\Lambda_b)$ value measured by the ATLAS Coll. was confirmed by the LHCb Coll. who found $R(\Lambda_b) = 0.513 \pm 0.023(\text{stat}) \pm 0.016(\text{syst}) \pm 0.011$ [43]. The small experimental rate ratio values are very puzzling since they imply decreasing $\Lambda_b \rightarrow \Lambda$ form factors for increasing q^2 -values in the charmonium mass region which is very counter-intuitive and contradicts all form factor models in the literature.

In Ref. [29] we again used the CCQM model to calculate invariant and helicity amplitudes for the transitions $\Lambda_b \rightarrow \Lambda^{(*)}(J^P) + J/\psi$ where the $\Lambda^{(*)}(J^P)$ are $\Lambda(s[ud])$ -type ground and excited states with J^P quantum numbers $J^P = \frac{1}{2}^\pm, \frac{3}{2}^\pm$. We found that the values of the helicity amplitudes for the $\Lambda^*(1520, \frac{3}{2}^-)$ and the $\Lambda^*(1890, \frac{1}{2}^-)$ are suppressed compared to those for the ground state $\Lambda(1116, \frac{1}{2}^+)$ and the excited state $\Lambda^*(1405, \frac{1}{2}^-)$. We emphasized that our analysis is important for the identification of the hidden charm pentaquark states P_c^+ which were discovered in the decay chain $\Lambda_b^0 \rightarrow P_c^+(\rightarrow pJ/\psi) + K^-$ by the LHCb Collaboration [44] because the cascade decay chain $\Lambda_b^0 \rightarrow \Lambda^*(\frac{3}{2}^\pm)(\rightarrow pK^-) + J/\psi$ involves the same final state.

In Ref. [30] we have made a comprehensive analysis of heavy-to-heavy and heavy-to-light nonleptonic heavy baryon two-body decays and have identified those decays that proceed solely via W -boson emission, i.e. via the tree graph contribution. Some sample decays are $\Omega_b^- \rightarrow \Omega_c^{(*)0}\rho^-(\pi^-)$, $\Omega_b^- \rightarrow \Omega^-J/\psi(\eta_c)$, $\Xi_b^{0,-} \rightarrow \Xi^{0,-}J/\psi(\eta_c)$, $\Lambda_b \rightarrow \Lambda J/\psi(\eta_c)$, $\Lambda_b \rightarrow \Lambda_c D_s^{(*)}$, $\Omega_c^- \rightarrow \Omega^- \rho^+(\pi^+)$ and $\Lambda_c \rightarrow p\phi$. We made use of the CCQM to calculate the tree graph contributions to these decays. We calculated rates, branching fractions and, for some of these decays, decay asymmetry parameters taking into account lepton mass effects. We compared our results to experimental results and the results of other theoretical approaches when they were available. Our main focus was on decays to final states with a lepton pair because of their clean experimental signature. For these decays we discussed two-fold polar angle decay distributions such as in the cascade decay $\Omega_b^- \rightarrow \Omega^-(\rightarrow \Xi\pi, \Lambda K^-) + J/\psi(\rightarrow \ell^+\ell^-)$.

In Ref. [31] we interpreted the new double charm baryon state found by the LHCb Collaboration in the invariant mass distribution of the set of final state particles ($\Lambda_c^+ K^- \pi^+ \pi^+$) as being at the origin of the decay chain $\Xi_{cc}^{++} \rightarrow \Sigma_c^{++} (\rightarrow \Lambda_c^+ \pi^+) + \bar{K}^{*0} (\rightarrow K^- \pi^+)$. The nonleptonic decay $\Xi_{cc}^{++} \rightarrow \Sigma_c^{++} + \bar{K}^{*0}$ belongs to a class of decays where the quark flavor composition is such that the decay proceeds solely via the factorizing tree-graph contribution precluding a contamination from W -exchange. We used the CCQM model to calculate the four helicity amplitudes that describe the dynamics of the transition $\Xi_{cc}^{++} \rightarrow \Sigma_c^{++}$ induced by the effective ($c \rightarrow u$) current. We then calculated the rate of the decay as well as the polarization of the Σ_c^{++} and Λ_c^+ daughter baryons and the longitudinal/transverse composition of the \bar{K}^{*0} . We estimated the decay $\Xi_{cc}^{++} \rightarrow \Sigma_c^{++} \bar{K}^{*0}$ to have a branching rate of $B(\Xi_{cc}^{++} \rightarrow \Sigma_c^{++} \bar{K}^{*0}) \sim 10.5\%$. As a byproduct of our investigation we have also analyzed the decay $\Xi_{cc}^{++} \rightarrow \Sigma_c^{++} \bar{K}^0$ for which we find a branching ratio of $B(\Xi_{cc}^{++} \rightarrow \Sigma_c^{++} \bar{K}^0) \sim 2.5\%$.

In Ref. [32] we performed an *ab initio* calculation of the W -exchange contribution to nonleptonic decays of double charm baryons Ξ_{cc}^{++} and Ω_{cc}^+ based on their three-quark structure. Preliminary approximate calculations [11,25,26] had indicated that the W -exchange contribution are not negligible. Prior to the above paper [32] there existed no first principles calculation of the W -exchange contribution. Again we used the CCQM model to calculate the tree graph contribution as well as the W -exchange contribution induced by diagram IIb. We calculated helicity amplitudes and determined the relative strengths of the two contributions to the helicity amplitudes. We found that the contribution of the W -exchange diagrams are suppressed in comparison with the tree-level contributions for the decay modes involving the flavor-symmetric final state charm baryon Ξ_c^+ . For the decay modes involving the flavor-antisymmetric final state charm baryon Ξ_c^+ the W -exchange contributions are not suppressed and even dominate over the tree-level contributions. We found that the W -exchange and tree diagram contributions are destructive for the decays into the Ξ_c^+ state. Finally, we compared the calculated decay widths with those from other theoretical approaches when they were available.

The main goal of our present paper is to provide a detailed description of our novel idea to calculate W -exchange diagrams occurring in nonleptonic decays of baryons (both light and heavy) in the context of our CCQM model which is based on the use of phenomenological nonlocal hadron-quark interaction Lagrangians.

The paper is structured as follows. In Sec. II we briefly review some basic notions of our CCQM model which are i) the underlying phenomenological nonlocal Lagrangians, ii) the implementation of hadronization and quark confinement, iii) the calculation of matrix elements, iv) the adjustment of the model parameters. We recount some important physical applications to the description of hadrons and their decays in our CCQM approach. In Sec. III we discuss our novel method of how to evaluate the W -exchange diagrams which involve the calculation of three-loop quark diagrams. We also discuss applications of our method to the nonleptonic decays of double charm baryons. In Sec. IV we present our numerical results for some specific nonleptonic decay modes of the double charm baryons $\Omega_{cc}^+ \rightarrow \Xi_c^+ (\Xi_c^+) + \bar{K}^0 (\bar{K}^{*0})$ and $\Xi_{cc}^{++} \rightarrow \Xi_c^+ (\Xi_c^+) + \pi^+ (\rho^+)$. Finally, in Sec. V, we summarize our results and present prospects for future studies.

2. Covariant Constituent Quark Model

In this section we describe the main features of the covariant constituent quark model (CCQM) [39–41] which will be used as a theoretical tool to address the hadron structure input in the study of nonleptonic decays of heavy baryons. The CCQM is a universal, truly relativistic, and a manifestly Lorentz covariant quark model for the description of hadrons as bound states of constituent quarks and of exotic states (hadronic molecules, tetraquarks, pentaquarks, hybrids, etc. [41,42]). Our approach allows one to study bound states with an arbitrary number of constituents and with arbitrary quantum numbers

(spin-parity, isospin, flavor content, etc.) The CCQM is based on a phenomenological, nonlocal relativistic Lagrangian describing the coupling of a hadron to its constituents. As an example we write down the Lagrangian describing the coupling of a baryon $B(q_1 q_2 q_3)$ to its three constituent quarks q_1 , q_2 , and q_3 . The Lagrangian has the form

$$\begin{aligned}\mathcal{L}_B(x) &= g_B \bar{B}(x) J_B(x) + \text{H.c.}, \\ J_B(x) &= \int dx_1 \int dx_2 \int dx_3 F_B(x; x_1, x_2, x_3) \varepsilon^{a_1 a_2 a_3} \Gamma_1 q^{a_1}(x_1) (q^{a_2}(x_2) C \Gamma_2 q^{a_3}(x_3)), \\ F_B(x; x_1, x_2, x_3) &= \delta^{(4)}\left(x - \sum_{i=1}^3 w_i x_i\right) \Phi_B\left(\sum_{i<j} (x_i - x_j)^2\right),\end{aligned}\quad (1)$$

where J_B is an interpolating three-quark current with the quantum numbers of the baryon state B . Further $w_i = m_i / (\sum_{j=1}^3 m_j)$ where m_i is the quark mass associated with the space-time point x_i . Γ_1 and Γ_2 are Dirac matrix strings. F_B is the Bethe-Salpeter kernel specifying the coupling of the baryon to the constituent quarks. The vertex form factor (or correlation function) Φ_B is a process-independent function which depends on the relative (Jacobi) coordinates and encodes the information concerning the distribution of the constituents in the bound state. A basic requirement for the choice of an explicit form of the correlation function Φ_B is that its Fourier transform vanishes sufficiently fast in the ultraviolet region of Euclidean space to render the Feynman diagrams ultraviolet finite.

Note that Eq. (1) is not the only possible choice that is compatible with Lorentz invariance. Any combination as $\sum_{i<j} (x_i - x_j)^2 / r_{ij}^2$ preserves both translational and Lorentz invariance. Generally speaking, the correlation r_{cd} should be different from r_{cc} . However, it will increase the number of adjustable parameters, i.e. one needs to keep different values for r_{cd} , r_{cs} and r_{cc} . But there is no much data even for the single-charmed baryon. The double-charmed baryon was discovered very recently by LHCb-collaboration. For that reasons, as a first approximation we equate the size parameter of double charm baryons with that of single charm baryons, i.e. we take $\Lambda_{cc} = \Lambda_c = 0.8675$ GeV where we adopt the value of Λ_c from [40].

For simplicity and calculational advantages we mostly adopt a Gaussian form for the correlation functions, i.e. we write

$$\begin{aligned}\Phi_B\left(\sum_{i<j} (x_i - x_j)^2\right) &= \int \frac{dq_1}{(2\pi)^4} \int \frac{dq_2}{(2\pi)^4} \tilde{\Phi}_B\left(-\frac{1}{2}(q_1 + q_2)^2 - \frac{1}{6}(q_1 - q_2)^2\right), \\ \tilde{\Phi}_B\left(-\vec{\Omega}^2\right) &= \exp\left(-\vec{\Omega}^2 / \Lambda_B^2\right)\end{aligned}\quad (2)$$

where Λ_B is the size parameter for a given baryon with values of the order of 1 GeV. The size parameter represents the extension of the distribution of the constituent quarks in the given baryon. The values of the size parameters Λ_B are fixed using data on fundamental properties of mesons and baryons such as leptonic decay constants, magnetic moments and radii. We emphasize that the Minkowskian momentum variable p^2 turns into the Euclidean form $-p_E^2$ needed for the appropriate fall-off behavior of the correlation function $\tilde{\Phi}_B$ in the Euclidean region. Any choice for the correlation function Φ_B is acceptable as long as it falls off sufficiently fast in the ultraviolet region of Euclidean space.

For given values of the size parameters Λ_B the coupling constant g_B is determined by the compositeness condition suggested by Weinberg and Salam [33,34] and extensively used in our approach. The compositeness condition implies that the renormalization constant of the hadron wave function is set equal to zero $Z_B = 1 - \Sigma'_B(m_B) = 0$, where Σ'_B is the on-shell derivative of the hadron mass function Σ_B

with respect to its momentum. The compositeness condition can be seen to provide for the correct charge normalization of a charged bound state.

Matrix elements of hadronic processes are computed in the S -matrix formalism, where the \hat{S} -operator is constructed from the interaction Lagrangian \mathcal{L}_{int}

$$\hat{S} = \hat{T} \exp \left[i \int d^4x \mathcal{L}_{\text{int}}(x) \right], \quad (3)$$

and where \hat{T} is the time-ordering operator. The Lagrangian \mathcal{L}_{int} includes two parts i) the model interaction Lagrangian which describes the coupling of hadrons to their constituent quarks (see Eq. (1)) which embodies the nonperturbative strong interaction effects at large distances and II) the electroweak part together with strong short-distance effects at the order of accuracy we are working in as given by the Standard Model (SM). As an illustration we consider the semileptonic decay $\Lambda_b^0 \rightarrow \Lambda_c^+ \ell^- \bar{\nu}_\ell$, which is described by the two-loop Feynman diagram shown in Fig. 2.

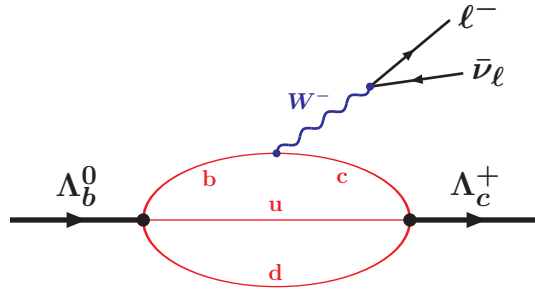


Figure 2. Feynman diagram describing the semileptonic decay $\Lambda_b^0 \rightarrow \Lambda_c^+ \ell^- \bar{\nu}_\ell$ decay.

The semileptonic weak Lagrangian describing the $b \rightarrow c \ell^- \bar{\nu}_\ell$ transition is given by

$$\mathcal{L}_{\text{sl}} = \frac{G_F}{\sqrt{2}} V_{cb} (\bar{c} O_\mu b) (\bar{\ell} O^\mu \nu_\ell), \quad O_\mu = \gamma_\mu (1 - \gamma_5), \quad (4)$$

where $G_F = 1.16638 \cdot 10^{-5} \text{ GeV}^{-2}$ is the Fermi constant, $V_{cb} = 0.0406$ the Cabibbo-Kobayashi-Maskawa matrix element.

The diagrams appearing in our approach can be viewed as ordinary Feynman diagrams in which the point-like particle-quark vertex functions are replaced by nonlocal vertex functions. Since the vertex functions enter as a building block in any given Feynman diagram it is clear that the nonlocal vertex functions are universal and not process dependent. As in ordinary Feynman diagrams one has free quark propagators $S_q(k) = 1/(m_q - \not{k})$ in terms of the constituent quark masses m_q with $q = u, d, s, c, b$. In particular, the invariant matrix element corresponding to the diagram in Fig. 2 is written as

$$\begin{aligned} \mathcal{M} &= \frac{G_F}{\sqrt{2}} V_{cb} g_{\Lambda_b} g_{\Lambda_c} \int \frac{d^4 k_1}{(2\pi)^4 i} \int \frac{d^4 k_2}{(2\pi)^4 i} \tilde{\Phi}_{\Lambda_b}(-\vec{\Omega}_{\text{in}}^2) \tilde{\Phi}_{\Lambda_c}(-\vec{\Omega}_{\text{out}}^2) \\ &\times \bar{u}_{\Lambda_c}(p') \Gamma_{\Lambda_c}^f S_c(k_1 + p') \Gamma_i S_b(k_1 + p) \Gamma_{\Lambda_b}^f u_{\Lambda_b}(p) \text{Tr} \left[\Gamma_{\Lambda_c}^i S_u(k_1 + k_2) \Gamma_{\Lambda_b}^i S_d(k_2) \right]. \end{aligned} \quad (5)$$

Γ_i is the set of Dirac matrices defining the $b \rightarrow c$ transition, $\Gamma_{\Lambda_c}^i, \Gamma_{\Lambda_c}^f$ and $\Gamma_{\Lambda_b}^i, \Gamma_{\Lambda_b}^f$ are the pair of Dirac matrices defining the spin structure of the Λ_c and Λ_b baryon, respectively, g_{Λ_c} and g_{Λ_b} are the coupling constants of Λ_c and Λ_b baryons with their constituent quarks. $\tilde{\Phi}_{\Lambda_c}$ and $\tilde{\Phi}_{\Lambda_b}$ are the Fourier transforms

of the correlation functions taking into account the distribution of quarks in the Λ_c and Λ_b baryons. The long-distance strong interaction effects are encoded in the correlation functions. The constituent quark masses $m_u = m_d = 0.241$ MeV, $m_s = 0.428$ GeV, $m_c = 1.672$ GeV and $m_b = 5.046$ GeV are taken to be universal for all processes considered in our formalism. Their values have been determined by a fit to a multitude of processes. The calculated matrix elements are expanded in terms of a set of relativistic form factors dictated by Lorentz and gauge invariance. It should be quite clear that the evaluation of the form factors is technically quite involved since it necessitates the calculation of two-loop Feynman diagrams with a complex spin structure resulting from the quark propagators and the vertex functions. The spin structure of the diagrams leads to a number of tensor integrals. To tackle this task we have automated the calculation in the form of FORM [45] and FORTRAN packages written for this purpose.

We emphasize that the CCQM model described here is a truly frame-independent field-theoretical quark model in contrast to other constituent quark models which are often quantum-mechanical with built-in relativistic elements. Also note that the HQET relations for the form factors can be recovered in the CCQM approach by using a $1/m_Q$ expansion for the heavy quark propagator. One of the advantages of the CCQM model is that it allows to calculate transition form factors in the full accessible range of momentum transfers. Heavy quark symmetry, for example, is expected to be reliable only close to zero recoil.

The local form of the quark propagators used in Eq. (5) can lead to unwanted singularities corresponding to free quark production in transition amplitudes, i.e. when $\sum m_{q_i} \leq m_B$. In a further refinement of earlier versions of our CCQM model we introduced effective infrared confinement by introducing a universal and finite scale variable, which, in the first version of the CCQM model without confinement, tends to infinity. The introduction of such an infrared cutoff removes all physical quark thresholds when $\sum m_{q_i} \leq m_B$. The CCQM model could thus be extended to cases where the hadron mass exceeded the sum of its constituents masses. The formalism was successfully applied to the decays of light and heavy mesons and baryons (see details in Refs. [39]).

In our papers the CCQM calculation of dynamical quantities in terms of e.g. helicity amplitudes was always accompanied by a model-independent derivation of the spin-kinematics of a given process. The ensuing angular decay distributions have been quite useful in the analysis of data and have been used by other theoretical and experimental groups (see e.g. discussion in Ref. [46]). In Table 1 we show some of our recent results on weak (semileptonic, radiative, and nonleptonic) decays of single and double heavy baryons and compare them to available data [1].

3. Nonleptonic decays of heavy baryons: Evaluation of the W -exchange diagrams

In this section we describe a novel method of how to evaluate the W -exchange contributions to the matrix elements of the nonleptonic decays of heavy baryons. In Table 2 we collect the quantum numbers of single and double charm baryons and define the interpolating currents that describe their nonlocal vertex structures.

As has been discussed before, nonleptonic baryonic two-body decays can be characterized by five types of topological color-flavor diagrams contributing to them (see Fig. 1). As an example we take the Cabibbo-favored nonleptonic decay modes of the spin-1/2 ground state double charm baryon states Ξ_{cc}^{++} , Ξ_{cc}^+ , Ω_{cc}^+ . In Table 3 we record which of the tree-level and W -exchange graphs contribute to a given single decay mode. It is noteworthy that eight of the fifteen flavor decay modes are contributed to only by W -exchange graphs.

Table 1. Branching ratios of weak decays of single and double heavy baryons (in %)

Mode	Our results	Data [1]
$\Lambda_c \rightarrow \Lambda e^+ \nu_e$	2.0	2.1 ± 0.6
$\Lambda_c \rightarrow \Lambda \mu^+ \nu_\mu$	2.0	2.0 ± 0.7
$\Lambda_c \rightarrow p \phi$	14.0	10.8 ± 1.4
$\Lambda_b \rightarrow \Lambda_c e^- \bar{\nu}_e$	6.6	$6.2^{+1.4}_{-1.3}$
$\Lambda_b \rightarrow \Lambda \mu^+ \mu^-$	1.0×10^{-4}	$(1.08 \pm 0.28) \times 10^{-4}$
$\Lambda_b \rightarrow \Lambda \gamma$	0.4×10^{-3}	< 0.13
$\Lambda_b^0 \rightarrow \Lambda_c^+ D_s^-$	147.8	110 ± 10
$\Lambda_b^0 \rightarrow \Lambda^0 J/\psi$	8.3	8.3 ± 1.1
$\Xi_{cc}^{++} \rightarrow \Sigma_c^{++} \bar{K}^{*0}$	5.4	
$\Xi_{cc}^{++} \rightarrow \Sigma_c^{++} \bar{K}^0$	1.3	
$\Xi_{cc}^{++} \rightarrow \Xi_c^+ \bar{\rho}^+$	16.7	
$\Xi_{cc}^{++} \rightarrow \Xi_c^+ \bar{\pi}^+$	0.3	
$\Xi_{cc}^{++} \rightarrow \Xi_c^+ \bar{\rho}^+$	0.2	
$\Xi_{cc}^{++} \rightarrow \Xi_c^+ \bar{\pi}^+$	0.1	

Table 2. Quantum numbers and interpolating currents of single and double charm baryons

Baryon	J^P	Interpolating current	Mass (MeV)
Ξ_{cc}^{++}	$\frac{1}{2}^+$	$\varepsilon_{abc} \gamma^\mu \gamma_5 u^a (c^b C \gamma_\mu c^c)$	3620.6
Ω_{cc}^+	$\frac{1}{2}^+$	$\varepsilon_{abc} \gamma^\mu \gamma_5 s^a (c^b C \gamma_\mu c^c)$	3710.0
Λ_c^+	$\frac{1}{2}^+$	$\varepsilon^{abc} c^a (u^b C \gamma_5 d^c)$	2286.46
Σ_c^{++}	$\frac{1}{2}^+$	$\varepsilon^{abc} \gamma^\mu \gamma_5 c^a (u^b C \gamma_\mu u^c)$	2453.97
Σ_c^+	$\frac{1}{2}^+$	$\varepsilon^{abc} \gamma^\mu \gamma_5 c^a (u^b C \gamma_\mu d^c)$	2452.9
Σ_c^0	$\frac{1}{2}^+$	$\varepsilon^{abc} \gamma^\mu \gamma_5 c^a (d^b C \gamma_\mu d^c)$	2453.75
Ξ_c^+	$\frac{1}{2}^+$	$\varepsilon^{abc} \gamma^\mu \gamma_5 c^a (u^b C \gamma_\mu s^c)$	2577.4
Ξ_c^0	$\frac{1}{2}^+$	$\varepsilon^{abc} \gamma^\mu \gamma_5 c^a (d^b C \gamma_\mu s^c)$	2577.9
Ξ_c^+	$\frac{1}{2}^+$	$\varepsilon_{abc} c^a (u^b C \gamma_5 s^c)$	2467.93
Ξ_c^0	$\frac{1}{2}^+$	$\varepsilon_{abc} c^a (d^b C \gamma_5 s^c)$	2470.85
Ω_c^0	$\frac{1}{2}^+$	$\varepsilon^{abc} \gamma^\mu \gamma_5 c^a (s^b C \gamma_\mu s^c)$	2695.2
Σ_c^{*++}	$\frac{3}{2}^+$	$\varepsilon^{abc} c^a (u^b C \gamma_\mu u^c)$	2518.41
Σ_c^{*+}	$\frac{3}{2}^+$	$\varepsilon^{abc} c^a (u^b C \gamma_\mu d^c)$	2517.5
Σ_c^{*0}	$\frac{3}{2}^+$	$\varepsilon^{abc} c^a (d^b C \gamma_\mu d^c)$	2518.481
Ξ_c^{*+}	$\frac{3}{2}^+$	$\varepsilon^{abc} c^a (u^b C \gamma_\mu s^c)$	2645.9
Ξ_c^{*0}	$\frac{3}{2}^+$	$\varepsilon^{abc} c^a (d^b C \gamma_\mu s^c)$	2645.9
Ω_c^{*0}	$\frac{3}{2}^+$	$\varepsilon^{abc} c^a (s^b C \gamma_\mu s^c)$	2765.9

Table 3. Classification of the Cabibbo favored nonleptonic two-body decays of the ground state double charm baryons

	I _a	I _b	II _a	II _b	III
$\Xi_{cc}^{++} \rightarrow \Sigma_c^{(*)++} + \bar{K}^{(*)0}$	-	√	-	-	-
$\Xi_{cc}^{++} \rightarrow \Xi_c^{(\prime,*)+} + \pi^+(\rho^+)$	√	-	-	√	-
$\Xi_{cc}^{++} \rightarrow \Sigma^{(*)+} + D^{(*)+}$	-	-	-	√	-
$\Xi_{cc}^+ \rightarrow \Xi_c^{(\prime,*)0} + \pi^+(\rho^+)$	√	-	√	-	-
$\Xi_{cc}^+ \rightarrow \Lambda_c^+(\Sigma_c^{(*)+}) + \bar{K}^{(*)0}$	-	√	√	-	-
$\Xi_{cc}^+ \rightarrow \Sigma_c^{(*)++} + K^{(*)-}$	-	-	√	-	-
$\Xi_{cc}^+ \rightarrow \Xi_c^{(\prime,*)+} + \pi^0(\rho^0)$	-	-	√	√	-
$\Xi_{cc}^+ \rightarrow \Xi_c^{(\prime,*)+} + \eta(\eta')$	-	-	√	√	-
$\Xi_{cc}^+ \rightarrow \Omega_c^{(*)0} + K^{(*)+}$	-	-	√	-	-
$\Xi_{cc}^+ \rightarrow \Lambda^0(\Sigma^{(*)0}) + D^{(*)+}$	-	-	-	√	√
$\Xi_{cc}^+ \rightarrow \Sigma^{(*)+} + D^{(*)0}$	-	-	-	-	√
$\Xi_{cc}^+ \rightarrow \Xi^{(*)0} + D_s^{(*)+}$	-	-	-	-	√
$\Omega_{cc}^+ \rightarrow \Xi_c^{(\prime,*)+} + \bar{K}^{(*)0}$	-	√	-	√	-
$\Omega_{cc}^+ \rightarrow \Xi^0(\prime,*) + D^{(*)+}$	-	-	-	√	-
$\Omega_{cc}^+ \rightarrow \Omega_c^0(\prime,*) + \pi^+(\rho^+)$	√	-	-	-	-

The Cabibbo-favored quark level nonleptonic transitions $\bar{s}c \rightarrow \bar{u}d$ are governed by the effective Hamiltonian

$$\begin{aligned}
\mathcal{H}_{\text{eff}} &= -g_{\text{eff}} (C_1 \mathcal{Q}_1 + C_2 \mathcal{Q}_2) + \text{H.c.}, \\
\mathcal{Q}_1 &= (\bar{s}_a O_L c_b)(\bar{u}_b O_L d_a) = (\bar{s}_a O_L d_a)(\bar{u}_b O_L c_b), \\
\mathcal{Q}_2 &= (\bar{s}_a O_L c_a)(\bar{u}_b O_L d_b) = (\bar{s}_a O_L d_b)(\bar{u}_b O_L c_a),
\end{aligned} \tag{6}$$

where we use the notation $g_{\text{eff}} = \frac{G_F}{\sqrt{2}} V_{cs} V_{ud}^\dagger$ and $O_L^\mu = \gamma^\mu(1 - \gamma_5)$ for the weak matrices with left chirality.

The color-flavor factor of the tree diagrams Ia and Ib depend on whether the emitted meson is charged or neutral. For charged emission the color-flavor factor is given by the combination of the Wilson coefficients $(C_2 + \zeta C_1)$, where $\zeta = 1/N_c$ and N_c is the number of colors, while for neutral emission the color-flavor factor reads $(C_1 + \zeta C_2)$. The W -exchange diagrams are more difficult to evaluate and will be the subject of the following paragraphs.

The nonlocal version of the interpolating currents shown in Table 3 reads

$$\begin{aligned}
J_{B_{cc}}(x) &= \int dx_1 \int dx_2 \int dx_3 F_{B_{cc}}(x; x_1, x_2, x_3) \varepsilon_{a_1 a_2 a_3} \gamma^\mu \gamma_5 q_{a_1}(x_1) (c_{a_2}(x_2) C \gamma_\mu c_{a_3}(x_3)) , \\
J_{B_c}(x) &= \int dx_1 \int dx_2 \int dx_3 F_{B_c}(x; x_1, x_2, x_3) \varepsilon_{a_1 a_2 a_3} \Gamma_1 c_{a_1}(x_1) (u_{a_2}(x_2) C \Gamma_2 s_{a_3}(x_3)) , \\
F_B &= \delta^{(4)}\left(x - \sum_{i=1}^3 w_i x_i\right) \Phi_B\left(\sum_{i<j}^3 (x_i - x_j)^2\right) ,
\end{aligned} \tag{7}$$

where we follow the notation introduced in Eq. (1).

In the following we shall restrict our discussion to the specific double charm baryon nonleptonic decay modes $\Xi_{cc}^{++} \rightarrow \Xi_c^{(\prime,*)+} + \pi^+(\rho^+)$ and $\Omega_{cc}^+ \rightarrow \Xi_c^{(\prime,*)+} + \bar{K}^{(*)0}$ studied in our most recent paper [32]. As Table 3 shows these decays obtain contributions from the tree diagram and the W -exchange topology IIb. The matrix element can be written as

$$\langle B_2 M | \mathcal{H}_{\text{eff}} | B_1 \rangle = g_{\text{eff}} \bar{u}(p_2) \left(12 C_T M_T + 12 (C_1 - C_2) M_W \right) u(p_1). \quad (8)$$

The tree diagram color factor for the neutral Ω_{cc}^+ decays is given by $C_T = -(C_1 + \zeta C_2)$ and by $C_T = +(C_2 + \zeta C_1)$ for the charged Ξ_{cc}^+ decays. The factor of $\zeta = 1/N_c$ is set to zero in our numerical calculations taking $N_c = \infty$. The overall factor of 12 in Eq. (8) has its origin in a combinatorial factor of 2 and a factor of 6 from the contraction of two Levi-Civita color tensors. The Feynman diagrams describing these processes are depicted in Fig. 3.

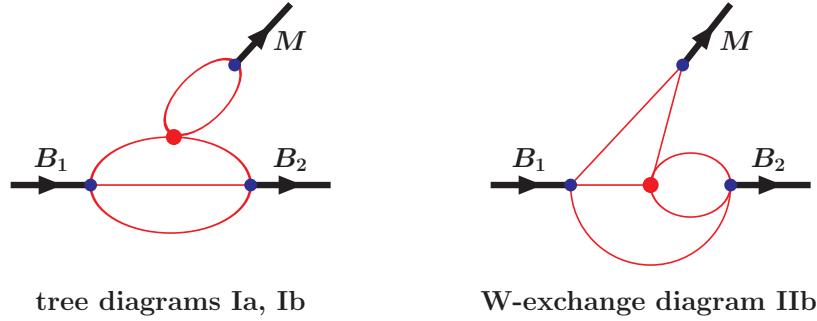


Figure 3. Pictorial representations of Eqs. (9) and (10).

The contribution from the tree diagram factorizes into two pieces according to

$$\begin{aligned} M_T &= M_T^{(1)} \cdot M_T^{(2)}, \\ M_T^{(1)} &= N_c g_M \int \frac{d^4 k}{(2\pi)^4 i} \tilde{\Phi}_M(-k^2) \text{tr} \left[O_L^\delta S_d(k - w_d q) \Gamma_M S_{s(u)}(k + w_{s(u)} q) \right] \\ M_T^{(2)} &= g_{B_1} g_{B_2} \int \frac{d^4 k_1}{(2\pi)^4 i} \int \frac{d^4 k_2}{(2\pi)^4 i} \tilde{\Phi}_{B_1}(-\vec{\Omega}_1^2) \tilde{\Phi}_{B_2}(-\vec{\Omega}_2^2) \\ &\quad \times \Gamma_1 S_c(k_2) \gamma^\mu S_c(k_1 - p_1) O_R^\delta S_{u(s)}(k_1 - p_2) \tilde{\Gamma}_2 S_{s(u)}(k_1 - k_2) \gamma_\mu \gamma_5. \end{aligned} \quad (9)$$

Here $\Gamma_1 \otimes \tilde{\Gamma}_2 = +I \otimes \gamma_5$ for the Ξ_c^+ -baryon and $-\gamma_\nu \gamma_5 \otimes \gamma^\nu$ for the $\Xi_c'^+$ -baryon.

The coupling constants g_M , g_{B_1} and g_{B_2} are determined by the compositeness condition as described in our previous papers (for details see, e.g. [30,31]). The Dirac matrix Γ_M in $M_T^{(1)}$ reads γ_5 and $\epsilon_V \cdot \gamma$ for the pseudoscalar meson P and for the vector meson V , respectively. The connection of $M_T^{(1)}$ with the leptonic decay constants $f_M = f_P, f_V$ is given by $M_T^{(1)} = -f_P q^\delta$ and $+f_V m_V \epsilon_V^\delta$. The minus sign in front of f_P appears because the momentum q flows in the opposite direction from the decay of P -meson.

The calculation of the three-loop W -exchange contribution is much more involved because the matrix element does not factorize. By using the Fierz transformation

$$O_{L/R}^{\alpha_1 \alpha_2} O_{R/L}^{\alpha_3 \alpha_4} = 2 (1 \pm \gamma_5)^{\alpha_1 \alpha_4} (1 \mp \gamma_5)^{\alpha_3 \alpha_2}$$

one has

$$\begin{aligned}
M_W &= g_{B_1} g_{B_2} g_M \int \frac{d^4 k_1}{(2\pi)^4 i} \int \frac{d^4 k_2}{(2\pi)^4 i} \int \frac{d^4 k_3}{(2\pi)^4 i} \tilde{\Phi}_{B_1}(-\vec{\Omega}_1^2) \tilde{\Phi}_{B_2}(-\vec{\Omega}_2^2) \tilde{\Phi}_M(-P^2) \\
&\times 2\Gamma_1 S_c(k_1) \gamma^\mu S_c(k_2) (1 - \gamma_5) S_d(k_2 - k_1 + p_2) \Gamma_M S_{s(u)}(k_2 - k_1 + p_1) \gamma_\mu \gamma_5 \\
&\times \text{tr} \left[S_{u(s)}(k_3) \tilde{\Gamma}_2 S_{s(u)}(k_3 - k_1 + p_2) (1 + \gamma_5) \right], \tag{10}
\end{aligned}$$

where $\Gamma_1 \otimes \tilde{\Gamma}_2 = I \otimes \gamma_5$ for $B_2 = \Xi_c^+$ and $-\gamma_\nu \gamma_5 \otimes \gamma^\nu$ for $B_2 = \Xi_c'^+$. Here $P = k_2 - k_1 + w_d p_1 + w_u p_2$ is the Jacobi momentum in the meson vertex function.

An important simplifying feature of the W -exchange contributions is a straightforward application of the Körner-Pati-Woo (KPW) theorem [47,48] which states that the contraction of a flavor-symmetric and flavor-antisymmetric configuration vanishes where the flavor-antisymmetric configuration follows from the $(V - A)(V - A)$ structure of the current-current interaction. In the present case the KPW theorem applies to the final state single charm baryon states $\Xi_c'^+$ and Ξ_c^{*+} built from a symmetric light flavor configuration ($c\{su\}$) which is contracted with the current-current vertex in the relevant topology Fig. IIb. One thus predicts that the Fig. IIb contribution to the decay modes $\Xi_{cc}^{++} \rightarrow \Xi_c^{(\prime,*)+} + \pi^+(\rho^+)$ and $\Omega_{cc}^+ \rightarrow \Xi_c^{(\prime,*)+} + \bar{K}^{(*)0}$ vanishes in the $SU(3)$ limit when $m_u = m_s$.

One can trace the working of the KPW theorem directly in our three-loop calculation. To do this, we change the order of Dirac matrices in the trace by using the properties of the charge conjugation matrix. Keeping in mind that γ_5 does not contribute to the trace, we have

$$\text{tr} \left[S_u(k_3) \gamma_\nu S_s(k_3 - k_1 + p_2) \right] = -\text{tr} \left[S_s(-k_3 + k_1 - p_2) \gamma_\nu S_u(-k_3) \right]. \tag{11}$$

We insert Eq. (11) into Eq. (10) and shift the integration variable $k_3 \rightarrow -k_3 + k_1 - p_2$. One can check that $\vec{\Omega}_2^2$ goes into itself under this transformation accompanied by an interchange of the u - and s -quark masses. Thus, if $m_u = m_s$ then the amplitude M_W is identical zero which directly confirms the KPW-theorem. We have checked numerically that the three-loop integral vanishes in this limit. $SU(3)$ breaking effects can be calculated by setting $m_u \neq m_s$.

Details of the calculation of the loop integrals and the subsequent reduction of the integration over Fock-Schwinger variables to an integration over a hypercube may be found in our previous papers (see e.g. the most recent papers [30,31]). Compared to the two-loop calculation of [30,31] we are now dealing with a three-loop calculation involving six quark propagators instead of the four propagators in the two-loop case. The calculation is quite time-consuming both analytically and numerically.

Next one expands the transition amplitudes in terms of invariant amplitudes. One has

$$\langle B_2 P | \mathcal{H}_{\text{eff}} | B_1 \rangle = g_{\text{eff}} \bar{u}(p_2) (A + \gamma_5 B) u(p_1), \tag{12}$$

$$\langle B_2 V | \mathcal{H}_{\text{eff}} | B_1 \rangle = g_{\text{eff}} \bar{u}(p_2) \epsilon_{V\delta}^* \left(\gamma^\delta V_\gamma + p_1^\delta V_p + \gamma_5 \gamma^\delta V_{5\gamma} + \gamma_5 p_1^\delta V_{5p} \right) u(p_1). \tag{13}$$

The invariant amplitudes are converted to a set of helicity amplitudes $H_{\lambda_1 \lambda_M}$ as described in [10]. One has

$$\begin{aligned}
H_{\frac{1}{2}^+}^V &= \sqrt{Q_+} A, & H_{\frac{1}{2}^+}^A &= \sqrt{Q_-} B, \\
H_{\frac{1}{2}^0}^V &= +\sqrt{Q_-/q^2} \left(m_+ V_\gamma + \frac{1}{2} Q_+ V_p \right), & H_{\frac{1}{2}^1}^V &= -\sqrt{2Q_-} V_\gamma, \\
H_{\frac{1}{2}^0}^A &= +\sqrt{Q_+/q^2} \left(m_- V_{5\gamma} + \frac{1}{2} Q_- V_{5p} \right), & H_{\frac{1}{2}^1}^A &= -\sqrt{2Q_+} V_{5\gamma},
\end{aligned} \tag{14}$$

where $m_{\pm} = m_1 \pm m_2$, $Q_{\pm} = m_{\pm}^2 - q^2$ and $|\mathbf{p}_2| = \lambda^{1/2}(m_1^2, m_2^2, q^2)/(2m_1)$. The helicities of the three particles are related by $\lambda_1 = \lambda_2 - \lambda_M$. We use the notation $\lambda_P = \lambda_t = 0$ for the scalar ($J = 0$) contribution in order to set the helicity label apart from $\lambda_V = 0$ used for the longitudinal component of the $J = 1$ vector meson. The remaining helicity amplitudes can be obtained from the parity relations $H_{-\lambda_2, -\lambda_M}^V = +H_{\lambda_2, \lambda_M}^V$ and $H_{-\lambda_2, -\lambda_M}^A = -H_{\lambda_2, \lambda_M}^A$. The helicity amplitudes have the dimension $[m]^3$. The numerical results on the helicity amplitudes given in Tables 4-7 are in units of GeV^3 .

The two-body decay widths read ($H_{\lambda_2 \lambda_M} = H_{\lambda_2 \lambda_M}^V - H_{\lambda_2 \lambda_M}^A$)

$$\Gamma(B_1 \rightarrow B_2 + P) = \frac{g_{\text{eff}}^2 |\mathbf{p}_2|}{16\pi m_1^2} \mathcal{H}_S, \quad \mathcal{H}_S = \left| H_{\frac{1}{2}t} \right|^2 + \left| H_{-\frac{1}{2}t} \right|^2, \quad (15)$$

$$\Gamma(B_1 \rightarrow B_2 + V) = \frac{g_{\text{eff}}^2 |\mathbf{p}_2|}{16\pi m_1^2} \mathcal{H}_V, \quad \mathcal{H}_V = \left| H_{\frac{1}{2}0} \right|^2 + \left| H_{-\frac{1}{2}0} \right|^2 + \left| H_{\frac{1}{2}1} \right|^2 + \left| H_{-\frac{1}{2}-1} \right|^2, \quad (16)$$

where we denote the sum of the squared moduli of the helicity amplitudes by \mathcal{H}_S and \mathcal{H}_V [30].

4. Numerical results

All model parameters have been fixed in our previous studies except for the size parameter Λ_{cc} of the double charmed baryons. As a first approximation we equate the size parameter of double charm baryons with that of single charm baryons, i.e. we take $\Lambda_{cc} = \Lambda_c = 0.8675 \text{ GeV}$ where we adopt the value of Λ_c from [40] obtained by fitting the magnetic moment of Λ_c to its experimental value.

Numerical results for the helicity amplitudes and decay widths are displayed in the Tables 4-7. In this review we concentrate on predictions for the rate values. In addition to the rate predictions, Tables 4-7 contain a wealth of spin polarization information. For example, for the decay $\Xi_{cc}^{++} \rightarrow \Xi_c^+ + \pi^+$ one finds an asymmetry parameter of $\alpha = -2H_{1/20}^V H_{1/20}^A / (|H_{1/20}^V|^2 + |H_{1/20}^A|^2) = -0.57$ while [18] predict a value in the range $\alpha = [-0.86, -1.00]$ depending on their model assumptions. Note that the W -exchange contribution in [18] is purely p -wave, i.e. proportional to $H_{1/20}^A$, due to the nonrelativistic approximations that they employ. This is in stark contrast to our relativistic result where the s -wave amplitude dominates in this process, i.e. $H_{1/20}^V / H_{1/20}^A = 3.3$. Both model calculations agree on a very substantial destructive interference of the tree and W -exchange contributions.

Our results highlight the importance of the KPW theorem for the nonleptonic decays when the final state involves a Ξ'^+ baryon containing a symmetric $\{su\}$ diquark. Tables 4-7 show that the relevant W -exchange contributions are nonzero but are strongly suppressed. Nonzero values result from $SU(3)$ breaking effects which are accounted for in our approach. Take for example the decay $\Xi_{cc}^{++} \rightarrow \Xi_c'^+ + \pi^+$. When compared to the tree contribution the $SU(3)$ breaking effects amount to $\sim (2 - 4)\%$. While the consequences of the KPW theorem for the W -exchange contribution are also incorporated in the pole model approach of [18] they are not included in the final-state interaction approach of [24].

In Table 8 we compare our rate results with the results of some other approaches [18,19,21,22,24,49]. For convenience purposes, we put the columns in orders corresponding to the number of calculated modes. We put Jiang et al. before Wang et al. according to alphabetical order. The rates calculated in [21] include tree graph contributions only. There is a wide spread in the rate values predicted by the various model calculations. All calculations approximately agree on the rate of the decay $\Xi_{cc}^{++} \rightarrow \Xi_c'^+ + \rho^+$ which is predicted to have a large branching ratio of $\sim 16\%$. In our calculation this mode is predicted to have by far the largest branching ratio of the decays analyzed in this paper. As concerns the decay $\Xi_{cc}^{++} \rightarrow \Xi_c^+ + \pi^+$ discovered by the LHCb Collaboration [9] we find a branching ratio of $\mathcal{B}(\Xi_{cc}^{++} \rightarrow \Xi_c^+ \pi^+) = 0.70\%$ using the central value of the life time measurement in [8]. The small value of the branching ratio results from a substantial cancellation of the tree and W -exchange contributions. The branching ratio is somewhat smaller than the branching ratio $\mathcal{B}(\Xi_{cc}^{++} \rightarrow \Sigma_c^{++} + \bar{K}^0) = 1.28\%$ calculated

in [31]. We think that the latter mode is more dominant in comparison with $\Xi_{cc}^{++} \rightarrow \Xi_c^+ \pi^+$. We predict a branching ratio considerably smaller than the range of branching fractions (6.66 – 15.79) % calculated in [18]. In our opinion the calculations done in Ref. [18] involve generous approximations for the errors which are hard to quantify.

An important issue is the accuracy of our results. The only free parameter in our approach is the size parameter Λ_{cc} of the double heavy baryons for which we have chosen $\Lambda_{cc} = 0.8675$ GeV in Tables 4-7. In order to estimate the uncertainty caused by the choice of the size parameter we allow the size parameter to vary from 0.6 to 1.135 GeV. We evaluate the mean $\bar{\Gamma} = \sum \Gamma_i / N$ and the mean square deviation $\sigma^2 = \sum (\Gamma_i - \bar{\Gamma})^2 / N$. The results for $N = 5$ are shown in Table 9. The rate errors amount to 6 – 15%. Since the dependence of the rates on Λ_{cc} is nonlinear the central values of the rates in Table 9 do not agree with the rate values in Tables 4-7.

Table 4. Decays $\Omega_{cc}^+ \rightarrow \Xi_c'^+ + \bar{K}^0 (\bar{K}^{*0})$

Helicity	Tree diagram	W diagram	total
$H_{\frac{1}{2}^+ t}^V$	0.20	-0.01	0.19
$H_{\frac{1}{2}^+ t}^A$	0.25	-0.01	0.24
$\Gamma(\Omega_{cc}^+ \rightarrow \Xi_c'^+ + \bar{K}^0) = 0.15 \cdot 10^{-13}$ GeV			
$H_{\frac{1}{2}^+ 0}^V$	-0.25	0.04×10^{-1}	-0.25
$H_{\frac{1}{2}^+ 0}^A$	-0.50	0.01	-0.49
$H_{\frac{1}{2}^+ 1}^V$	0.27	-0.01	0.26
$H_{\frac{1}{2}^+ 1}^A$	0.56	0.04×10^{-2}	0.56
$\Gamma(\Omega_{cc}^+ \rightarrow \Xi_c'^+ + \bar{K}^{*0}) = 0.74 \cdot 10^{-13}$ GeV			

Table 6. Decays $\Xi_{cc}^{++} \rightarrow \Xi_c'^+ + \pi^+ (\rho^+)$

Helicity	Tree diagram	W diagram	total
$H_{\frac{1}{2}^+ t}^V$	-0.38	-0.01	-0.39
$H_{\frac{1}{2}^+ t}^A$	-0.55	-0.02	-0.57
$\Gamma(\Xi_{cc}^{++} \rightarrow \Xi_c'^+ + \pi^+) = 0.82 \cdot 10^{-13}$ GeV			
$H_{\frac{1}{2}^+ 0}^V$	0.60	0.04×10^{-1}	0.61
$H_{\frac{1}{2}^+ 0}^A$	1.20	0.01	1.21
$H_{\frac{1}{2}^+ 1}^V$	-0.49	-0.01	-0.50
$H_{\frac{1}{2}^+ 1}^A$	-1.27	0.01×10^{-1}	-1.27
$\Gamma(\Xi_{cc}^{++} \rightarrow \Xi_c'^+ + \rho^+) = 4.27 \cdot 10^{-13}$ GeV			

Table 5. Decays $\Omega_{cc}^+ \rightarrow \Xi_c^+ + \bar{K}^0 (\bar{K}^{*0})$

Helicity	Tree diagram	W diagram	total
$H_{\frac{1}{2}^+ t}^V$	-0.35	1.06	0.71
$H_{\frac{1}{2}^+ t}^A$	-0.10	0.31	0.21
$\Gamma(\Omega_{cc}^+ \rightarrow \Xi_c^+ + \bar{K}^0) = 0.95 \cdot 10^{-13}$ GeV			
$H_{\frac{1}{2}^+ 0}^V$	0.50	-0.69	-0.19
$H_{\frac{1}{2}^+ 0}^A$	0.18	-0.45	-0.27
$H_{\frac{1}{2}^+ 1}^V$	-0.11	-0.24	-0.35
$H_{\frac{1}{2}^+ 1}^A$	-0.18	0.66	0.48
$\Gamma(\Omega_{cc}^+ \rightarrow \Xi_c^+ + \bar{K}^{*0}) = 0.62 \cdot 10^{-13}$ GeV			

Table 7. Decays $\Xi_{cc}^{++} \rightarrow \Xi_c^+ + \pi^+ (\rho^+)$

Helicity	Tree diagram	W diagram	total
$H_{\frac{1}{2}^+ t}^V$	-0.70	0.99	0.29
$H_{\frac{1}{2}^+ t}^A$	-0.21	0.30	0.09
$\Gamma(\Xi_{cc}^{++} \rightarrow \Xi_c^+ + \pi^+) = 0.18 \cdot 10^{-13}$ GeV			
$H_{\frac{1}{2}^+ 0}^V$	1.17	-0.70	0.47
$H_{\frac{1}{2}^+ 0}^A$	0.45	-0.44	0.003
$H_{\frac{1}{2}^+ 1}^V$	-0.20	-0.23	-0.43
$H_{\frac{1}{2}^+ 1}^A$	-0.41	0.62	0.21
$\Gamma(\Xi_{cc}^{++} \rightarrow \Xi_c^+ + \rho^+) = 0.63 \cdot 10^{-13}$ GeV			

5. Summary and outlook

We have proposed a calculational technique which allows one to evaluate the W -exchange graphs in nonleptonic decays of heavy and light baryons. In this review we have concentrated on the description of Cabibbo-favored nonleptonic two-body decays of the double charm ground state baryons Ξ_{cc}^{++} , Ξ_{cc}^+ , and Ω_{cc}^+ where we have limited our analysis to the $1/2^+ \rightarrow 1/2^+ + P(V)$ decay channels. It would be straightforward to also include the $1/2^+ \rightarrow 3/2^+ + P(V)$ nonleptonic decays not discussed in this review. Also the study could be extended to the description of singly and doubly suppressed Cabibbo decays not only for double charm baryon decays but also for single charm baryon decays. In the future we plan to extend our predictions for other modes of nonleptonic decays of double and single heavy baryons taking

Table 8. Comparison with other approaches. Abbreviation: M=NRQM, T=HQET

Mode	Width (in 10^{-13} GeV)					
	GIKLT [31,32]	DS [18,19]	JHL [24]	WYZ [21]	YJLLWZ [49]	KL [22]
$\Xi_{cc}^{++} \rightarrow \Sigma_c^{++} + \bar{K}^0$	0.33					
$\Xi_{cc}^{++} \rightarrow \Sigma_c^{++} + \bar{K}^{*0}$	1.38					
$\Omega_{cc}^+ \rightarrow \Xi_c'^+ + \bar{K}^0$	0.15	0.31 (M) 0.59 (T)				
$\Omega_{cc}^+ \rightarrow \Xi_c^+ + \bar{K}^0$	0.95	0.68 (M) 1.08 (T)				
$\Omega_{cc}^+ \rightarrow \Xi_c'^+ + \bar{K}^{*0}$	0.74		$2.64^{+2.72}_{-1.79}$			
$\Omega_{cc}^+ \rightarrow \Xi_c^+ + \bar{K}^{*0}$	0.62		$1.38^{+1.49}_{-0.95}$			
$\Xi_{cc}^{++} \rightarrow \Xi_c'^+ + \pi^+$	0.82	1.40 (M) 1.93 (T)		1.10		
$\Xi_{cc}^{++} \rightarrow \Xi_c^+ + \pi^+$	0.18	1.71 (M) 2.39 (T)		1.57	1.58	2.25
$\Xi_{cc}^{++} \rightarrow \Xi_c'^+ + \rho^+$	4.27		$4.25^{+0.32}_{-0.19}$	4.12	3.82	
$\Xi_{cc}^{++} \rightarrow \Xi_c^+ + \rho^+$	0.63		$4.11^{+1.37}_{-0.86}$	3.03	2.76	6.70

Table 9. Estimating uncertainties in the decay widths.

Mode	Width (in 10^{-13} GeV)
$\Omega_{cc}^+ \rightarrow \Xi_c'^+ + \bar{K}^0$	0.14 ± 0.01
$\Omega_{cc}^+ \rightarrow \Xi_c'^+ + \bar{K}^{*0}$	0.72 ± 0.06
$\Omega_{cc}^+ \rightarrow \Xi_c^+ + \bar{K}^0$	0.87 ± 0.13
$\Omega_{cc}^+ \rightarrow \Xi_c^+ + \bar{K}^{*0}$	0.58 ± 0.07
$\Xi_{cc}^{++} \rightarrow \Xi_c'^+ + \pi^+$	0.77 ± 0.05
$\Xi_{cc}^{++} \rightarrow \Xi_c'^+ + \rho^+$	4.08 ± 0.29
$\Xi_{cc}^{++} \rightarrow \Xi_c^+ + \pi^+$	0.16 ± 0.02
$\Xi_{cc}^{++} \rightarrow \Xi_c^+ + \rho^+$	0.59 ± 0.04

into account W -exchange contributions. One can see from our analysis that the W -exchange contributions are generally not suppressed. Moreover, one can identify decay modes that are contributed to only by W -exchange graphs. A typical example is the doubly Cabibbo-suppressed decay $\Xi_c^+ \rightarrow p\phi$ recently observed by the LHCb Collaboration [50] which is induced by the quark level transition ($c \rightarrow d$; $s \rightarrow u$). In our classification it is contributed to by the topology diagram IIb.

Funding: This work was funded by the Carl Zeiss Foundation under Project “Kepler Center für Astro- und Teilchenphysik: Hochsensitive Nachweistechnik zur Erforschung des unsichtbaren Universums (Gz: 0653-2.8/581/2)”, by CONICYT (Chile) PIA/Basal FB0821. M.A.I. acknowledges the support from the PRISMA⁺ Cluster of Excellence (Mainz Uni.). M.A.I. and J.G.K. acknowledge the support of a Heisenberg-Landau grant.

Conflicts of Interest: The authors declare no conflict of interest

References

1. M. Tanabashi *et al.* (Particle Data Group), *Phys. Rev. D* **2018**, *98*, 030001.
2. M. Ablikim *et al.* (BESIII Collaboration), *Phys. Rev. Lett.* **2016**, *116*, 052001.
3. Y. B. Li *et al.* [Belle Collaboration], arXiv:1904.12093 [hep-ex].
4. V. M. Abazov *et al.* [D0 Collaboration], *Phys. Rev. D* **2011**, *84*, 031102.
5. G. Aad *et al.* (ATLAS Collaboration), *Phys. Lett. B* **2015**, *751*, 63.
6. A. Ocherashvili *et al.* (SELEX Collaboration), *Phys. Lett. B* **2005**, *628*, 18.
7. R. Aaij *et al.* (LHCb Collaboration), *Phys. Rev. Lett.* **2017**, *119*, 112001.
8. R. Aaij *et al.* (LHCb Collaboration), *Phys. Rev. Lett.* **2018**, *121*, 052002.
9. R. Aaij *et al.* (LHCb Collaboration), *Phys. Rev. Lett.* **2018**, *121*, 162002.
10. J. G. Körner and M. Krämer, *Z. Phys. C* **1992**, *55*, 659.
11. J. G. Körner, M. Krämer and D. Pirjol, *Prog. Part. Nucl. Phys.* **1994**, *33*, 787.
12. A. De Rujula, H. Georgi and S. L. Glashow, *Phys. Rev. D* **1975**, *12*, 3589.
13. D. Ebert, R. N. Faustov, V. O. Galkin and A. P. Martynenko, *Phys. Rev. D* **2002**, *66*, 014008.
14. S. Fleck and J. M. Richard, *Prog. Theor. Phys.* **1989**, *82*, 760.
15. M. Karliner and J. L. Rosner, *Phys. Rev. D* **2014**, *90*, 094007.
16. J. G. Körner, G. Kramer and J. Willrodt, *Z. Phys. C* **1979**, *2*, 117.
17. A. K. Leibovich, Z. Ligeti, I. W. Stewart and M. B. Wise, *Phys. Lett. B* **2004**, *586*, 337.
18. N. Sharma and R. Dhir, *Phys. Rev. D* **2017**, *96*, 113006.
19. R. Dhir and N. Sharma, *Eur. Phys. J. C* **2018**, *78*, 743.
20. Q. A. Zhang, *Eur. Phys. J. C* **2018**, *78*, 1024.
21. W. Wang, F. S. Yu and Z. X. Zhao, *Eur. Phys. J. C* **2017**, *77*, 781.
22. V. V. Kiselev and A. K. Likhoded, *Phys. Usp.* **2002**, *45*, 455 [*Usp. Fiz. Nauk* **2002**, *172*, 497].
23. A. V. Berezhnoy, A. K. Likhoded and A. V. Luchinsky, *Phys. Rev. D* **2018**, *98*, 113004.
24. L. J. Jiang, B. He and R. H. Li, *Eur. Phys. J. C* **2018**, *78*, 961.
25. M. A. Ivanov, J. G. Körner, V. E. Lyubovitskij and A. G. Rusetsky, *Phys. Rev. D* **1998**, *57*, 5632.
26. M. A. Ivanov, J. G. Körner, V. E. Lyubovitskij and A. G. Rusetsky, *Mod. Phys. Lett. A* **1998**, *13*, 181.
27. T. Gutsche, M. A. Ivanov, J. G. Körner, V. E. Lyubovitskij and P. Santorelli, *Phys. Rev. D* **2013**, *88*, 114018.
28. T. Gutsche, M. A. Ivanov, J. G. Körner, V. E. Lyubovitskij and P. Santorelli, *Phys. Rev. D* **2015**, *92*, 114008.
29. T. Gutsche, M. A. Ivanov, J. G. Körner, V. E. Lyubovitskij, V. V. Lyubushkin and P. Santorelli, *Phys. Rev. D* **2017**, *96*, 013003.
30. T. Gutsche, M. A. Ivanov, J. G. Körner and V. E. Lyubovitskij, *Phys. Rev. D* **2018**, *98*, 074011.
31. T. Gutsche, M. A. Ivanov, J. G. Körner and V. E. Lyubovitskij, *Phys. Rev. D* **2017**, *96*, 054013.
32. T. Gutsche, M. A. Ivanov, J. G. Körner, V. E. Lyubovitskij and Z. Tyulemissov, *Phys. Rev. D* **2019**, *99*, 056013.
33. A. Salam, *Nuovo Cim.* **1962**, *25*, 224.
34. S. Weinberg, *Phys. Rev.* **1963**, *130*, 776.
35. K. Hayashi, M. Hirayama, T. Muta, N. Seto and T. Shirafuji, *Fortsch. Phys.* **1967**, *15*, 625.

36. G. V. Efimov and M. A. Ivanov, *The Quark Confinement Model of Hadrons*, (IOP Publishing, Bristol & Philadelphia, 1993).
37. M. A. Ivanov, M. P. Locher and V. E. Lyubovitskij, *Few Body Syst.* **1996**, 21, 131; M. A. Ivanov, V. E. Lyubovitskij, J. G. Körner and P. Kroll, *Phys. Rev. D* **1997**, 56, 348; M. A. Ivanov, J. G. Körner, V. E. Lyubovitskij and A. G. Rusetsky, *Phys. Lett. B* **1998**, 442, 435; *Phys. Rev. D* **1999**, 60, 094002; A. Faessler, T. Gutsche, M. A. Ivanov, J. G. Körner and V. E. Lyubovitskij, *Phys. Lett. B* **2001**, 518, 55; A. Faessler, T. Gutsche, M. A. Ivanov, J. G. Körner and V. E. Lyubovitskij, *Eur. Phys. J. direct* **2002**, 4, 18; A. Faessler, T. Gutsche, M. A. Ivanov, V. E. Lyubovitskij and P. Wang, *Phys. Rev. D* **2003**, 68, 014011; A. Faessler, T. Gutsche, M. A. Ivanov, J. G. Körner, V. E. Lyubovitskij, D. Nicmorus and K. Pumsa-ard, *Phys. Rev. D* **2006**, 73, 094013; A. Faessler, T. Gutsche, M. A. Ivanov, J. G. Körner and V. E. Lyubovitskij, *Phys. Rev. D* **2009**, 80, 034025; T. Branz, A. Faessler, T. Gutsche, M. A. Ivanov, J. G. Körner, V. E. Lyubovitskij and B. Oexl, *Phys. Rev. D* **2010**, 81, 114036.
38. M. A. Ivanov and P. Santorelli, *Phys. Lett. B* **1999**, 456, 248; M. A. Ivanov, J. G. Körner and P. Santorelli, *Phys. Rev. D* **63**, 074010 (2001). *Phys. Rev. D* **2005**, 71, 094006; *Phys. Rev. D* **2007**, 75, 019901(E).
39. T. Branz, A. Faessler, T. Gutsche, M. A. Ivanov, J. G. Körner and V. E. Lyubovitskij, *Phys. Rev. D* **2010**, 81, 034010; M. A. Ivanov, J. G. Körner, S. G. Kovalenko, P. Santorelli and G. G. Saidullaeva, *Phys. Rev. D* **2012**, 85, 034004; T. Gutsche, M. A. Ivanov, J. G. Körner, V. E. Lyubovitskij and P. Santorelli, *Phys. Rev. D* **2013**, 87, 074031; T. Gutsche, M. A. Ivanov, J. G. Körner, V. E. Lyubovitskij and P. Santorelli, *Phys. Rev. D* **2014**, 90, 114033; *Phys. Rev. D* **2016**, 94, 059902(E); T. Gutsche, M. A. Ivanov, J. G. Körner, V. E. Lyubovitskij, P. Santorelli and N. Habył, *Phys. Rev. D* **2015**, 91, 074001; *Phys. Rev. D* **2015**, 91, 119907(E); C. T. Tran, M. A. Ivanov, J. G. Körner and P. Santorelli, *Phys. Rev. D* **2018**, 97, 054014.
40. T. Gutsche, M. A. Ivanov, J. G. Körner, V. E. Lyubovitskij and P. Santorelli, *Phys. Rev. D* **2016**, 93, 034008.
41. S. Dubnicka, A. Z. Dubnickova, M. A. Ivanov and J. G. Körner, *Phys. Rev. D* **2010**, 81, 114007; S. Dubnicka, A. Z. Dubnickova, M. A. Ivanov, J. G. Körner, P. Santorelli and G. G. Saidullaeva, *Phys. Rev. D* **2011**, 84, 014006; T. Gutsche, M. A. Ivanov, J. G. Körner and V. E. Lyubovitskij, *Phys. Rev. D* **2016**, 94, 094012; F. Goerke, T. Gutsche, M. A. Ivanov, J. G. Körner, V. E. Lyubovitskij and P. Santorelli, *Phys. Rev. D* **2016**, 94, 094017; F. Goerke, T. Gutsche, M. A. Ivanov, J. G. Körner and V. E. Lyubovitskij, *Phys. Rev. D* **2017**, 96, 054028; T. Gutsche, M. A. Ivanov, J. G. Körner, V. E. Lyubovitskij and K. Xu, *Phys. Rev. D* **2017**, 96, 114004.
42. A. Faessler, T. Gutsche, V. E. Lyubovitskij and Y. L. Ma, *Phys. Rev. D* **2007**, 76, 014005; *Phys. Rev. D* **2007**, 76, 114008; Y. Dong, A. Faessler, T. Gutsche, S. Kovalenko and V. E. Lyubovitskij, *Phys. Rev. D* **2008**, 77, 094013; *Phys. Rev. D* **2009**, 79, 094013; T. Branz, T. Gutsche and V. E. Lyubovitskij, *Phys. Rev. D* **2009**, 80, 054019; Y. Dong, A. Faessler, T. Gutsche and V. E. Lyubovitskij, *J. Phys. G* **2011**, 38, 015001; *Phys. Rev. D* **2013**, 88, 014030.
43. R. Aaij *et al.* (LHCb Collaboration), *JHEP* **2019**, 1903, 126.
44. R. Aaij *et al.* (LHCb Collaboration), *Phys. Rev. Lett.* **2015**, 115, 072001M *Phys. Rev. Lett.* **2016**, 117, 082002; arXiv:1904.03947 [hep-ex].
45. J. A. M. Vermaseren, *Nucl. Phys. Proc. Suppl.* **2008**, 183, 19; J. A. M. Vermaseren, *New features of FORM*, math-ph/0010025.
46. S. Meinel, *PoS LATTICE* **2014**, 2013, 024; *Phys. Rev. D* **2012**, 86, 010001.
47. J. G. Körner, *Nucl. Phys. B* **1971**, 25, 282.
48. J. C. Pati and C. H. Woo, *Phys. Rev. D* **1971**, 3, 2920.
49. F. S. Yu, H. Y. Jiang, R. H. Li, C. D. Lü, W. Wang and Z. X. Zhao, *Chin. Phys. C* **2018**, 42, 051001.
50. R. Aaij *et al.* [LHCb Collaboration], *JHEP* **2019**, 1904, 084.